

# Phase Retrieval for Partially Coherent Observations

Jonas Kornprobst, *Student Member, IEEE*, Alexander Paulus, *Student Member, IEEE*,  
Josef Knapp, *Student Member, IEEE*, and Thomas F. Eibert, *Senior Member, IEEE*

**Abstract**—Phase retrieval is in general a non-convex and non-linear task and the corresponding algorithms struggle with the issue of local minima. We consider the case where the measurement samples within typically very small and disconnected subsets are coherently linked to each other—which is a reasonable assumption for our objective of antenna measurements. Two classes of measurement setups are discussed which can provide this kind of extra information: multi-probe systems and holographic measurements with multiple reference signals. We propose several formulations of the corresponding phase retrieval problem. The simplest of these formulations poses a linear system of equations similar to an eigenvalue problem where a unique non-trivial null-space vector needs to be found. Accurate phase reconstruction for partially coherent observations is, thus, possible by a reliable solution process and with judgment of the solution quality. Under ideal, noise-free conditions, the required sampling density is less than two times the number of unknowns. Noise and other observation errors increase this value slightly. Simulations for Gaussian random matrices and for antenna measurement scenarios demonstrate that reliable phase reconstruction is possible with the presented approach.

**Index Terms**—linear phase retrieval, non-convex non-linear cost function minimization, magnitude-only near-field far-field transformation, equivalent source reconstruction

## I. INTRODUCTION

PHASE RETRIEVAL is a type of inverse problem arising in many research fields, including optics [1], [2], X-ray crystallography [3], [4], high-frequency engineering [5]–[8], transmission electron microscopy [9], [10], coherent diffraction imaging [11]–[13] and ptychography [14]–[16]. From a mathematical point of view, the behavior of phase retrieval algorithms is often studied for abstract scenarios, e.g., Gaussian random matrices, to develop new solution strategies, since this allows to (statistically) analyze the convergence behavior of the algorithms [17]–[24].

For other than random Gaussian matrices, phase retrieval can not be proven to work with absolute certainty, or absolute certainty can only be attained for unrealistic measurement accuracies and with quadratic oversampling rates [8]. Hence, a rather popular strategy is to integrate additional information into the problem formulation, going beyond magnitude-only measurements. If feasible, one may change the observation kernel (masking [25], exploitation of multiple measurement distances [5], [6], [26]) or enforce sparsity [27]–[31]. Another way is to relax the original assumption of magnitude-only observations to some extent.

J. Kornprobst, A. Paulus, J. Knapp and T. F. Eibert are with the Chair of High-Frequency Engineering, Department of Electrical and Computer Engineering, Technical University of Munich, 80290 Munich, Germany (e-mail: j.kornprobst@tum.de, hft@ei.tum.de).

This work was supported by the German Federal Ministry for Economic Affairs and Energy under Grant 50RK1923.

In this work, we consider the case where (possibly small) subsets of the total observations are captured coherently. In antenna measurements, this can be achieved with special multi-probe or multi-frequency measurements [7], [32]–[38]. In optics, measurements with specialized masks containing structured modulations can be seen as multi-probe measurements [39]. A similar problem arises in holography for the stitching of holographic images, where the relation between reference signal (from a reference antenna or beam) and measurement signal is changed. Examples of holographic antenna measurement techniques are found in [40]–[47] and of optical holography in [48]–[50]. Angular synchronization [51]–[53] or phase unwrapping [54], [55] are similar but different.

The phase differences obtained from such measurements are typically disconnected and many phase differences needed for straightforward phase reconstruction by concatenation are missing. Thus, the determination of the absolute phases at all the measurement locations remains a non-trivial phase retrieval problem. In order to solve the phase-retrieval problem by the concatenation of phase differences, the observations need to be collected in an appropriate manner [33]. Due to practical restrictions related to positioning accuracy and error concatenation, such an approach is only of limited utility.

We do not restrict our investigations to the special case of near-field (NF) antenna measurements and propose several general formulations of the magnitude-only inverse problem with partially coherent observations together with related solution strategies. With sufficiently oversampled observations and suitable forward operator properties, we show that the phase retrieval problem even becomes linear. The formulations are applicable to any kind of phase retrieval where partially coherent observations are available. The great advantage is that the search for the global minimum—even under the influence of measurement errors—becomes feasible. Phase retrieval results for synthetic data, noisy and ideal, demonstrate that a solution as close as possible to the true one can be reconstructed with certainty, once the corresponding sampling limit is reached—given that mild conditions on the forward operator of the inverse problem are fulfilled.

The paper is structured as follows. Section II introduces the magnitude-only inverse problem. Several formulations for phase retrieval with partially coherent observations are proposed in Section III. Section IV demonstrates the applicability to random complex matrices and illustrates the limitations of all variants. Furthermore, we investigate a possible way of how to incorporate the method into NF far-field (FF) transformations (NFFFTs) with special multi-element probes.



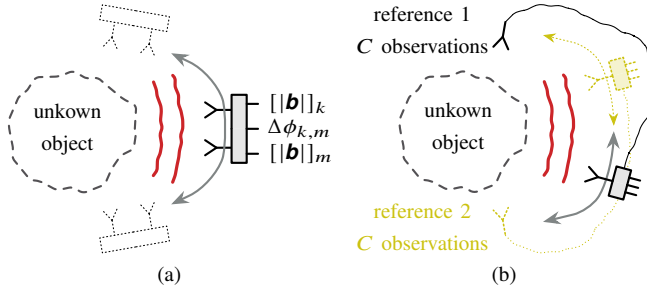


Figure 2. Electromagnetic measurement setups for partially coherent observations. (a) A multi-probe approach,  $C = 2$ . (b) A holographic approach with two coherent data sets,  $M = 2$  and  $C$  is large.

are limited to solving non-convex non-linear minimization problems [7], [36] or they utilize restrictive—*unrealistic or even unfeasible*—sampling strategies [33], [36], [56].

In the general case, the forward matrix is  $\mathbf{A} \in \mathbb{C}^{CM \times N}$ , the magnitude-only observation vector is  $|\mathbf{b}| \in \mathbb{R}^{CM}$ , and the phase unknowns vector is  $\boldsymbol{\phi} \in \mathbb{C}^{CM}$ . The inverse problem

$$\begin{aligned} \min_{\boldsymbol{\phi}, \mathbf{x}} \quad & \|\mathbf{A}\mathbf{x} - \text{diag}(\boldsymbol{\phi})|\mathbf{b}|\|_2 \\ \text{s. t.} \quad & |[\boldsymbol{\phi}]_m| = 1 \quad \text{for } m \in \mathbb{N}^{[1, CM]} \\ & \frac{[\boldsymbol{\phi}]_{m+cM}}{[\boldsymbol{\phi}]_m} = e^{j\Delta\phi_{m+cM,m}} \quad \text{for } m \in \mathbb{N}^{[1, M]} \\ & \text{and for } c \in \mathbb{N}^{[1, C-1]} \end{aligned} \quad (6)$$

is now additionally constrained by the observed phase differences  $\Delta\phi_{m+cM,m}$ . Alternatively, we can state that the phase differences  $\Delta\phi_{k,m}$  according to (5) are only observed if  $\text{mod}(k - m, M) = 0$ . These phase differences do *not* carry the same information as the standard complex data, since they are fewer in number and concatenation is not possible—for instance, the phase differences from the first subset of  $C$  observations  $m = \{1, M + 1, 2M + 1, \dots, (C - 1)M + 1\}$  to any other observation outside this subset are missing.

Let us emphasize the key aspect that there are now  $CM$  magnitude-only observations and  $(C - 1)M$  coherent and linearly independent phase-difference observations. Simple concatenation of the phase differences is not feasible as  $M - 1$  phase differences plus a global phase are still unknown. Since the standard phase retrieval problem (3) is augmented in (6), we expect the minimum number of observations  $CM$  for successful reconstruction in the range  $N \leq CM \leq 4N$ , with the approximate empirical upper bound  $4N$  for standard phase retrieval [19].

### B. Possible Phase-Difference Measurement Techniques

Let us consider two basic types of measurement scenarios: i) multi-probe systems, see Fig. 2(a), and ii) holographic systems with multiple reference signals, see Fig. 2(b), where reciprocal permutations are possible (the reference may be on the transmitting or receiving side). Fig. 2 focuses on antenna measurement systems; comparable systems in optics have been mentioned in the introduction.

The first case of multi-probe observations seems more challenging since  $C$  is typically rather small, e.g.,  $C = 2$

in [7], [32]–[35]. In such a scenario, very small (localized) and possibly unconnected “isles” of coherent observations are taken everywhere on the measurement surface of interest, which is feasible in two ways. The particular phase differences of interest are observed either directly by multi-channel receivers with shared oscillator signals or via distinct magnitude observations in the form of  $|\mathbf{b}|_k$ ,  $|\mathbf{b}|_m$ ,  $|\mathbf{b}|_k + |\mathbf{b}|_m$ ,  $|\mathbf{b}|_k + j|\mathbf{b}|_m$ , which allows to numerically reconstruct the phase differences as

$$\Delta\phi_{k,m} = \text{atan} \frac{|\mathbf{b}|_k + |\mathbf{b}|_m|^2 - |\mathbf{b}|_k|^2 - |\mathbf{b}|_m|^2}{|\mathbf{b}|_k + j|\mathbf{b}|_m|^2 - |\mathbf{b}|_k|^2 - |\mathbf{b}|_m|^2}. \quad (7)$$

Other sets of at least four linear combinations of  $|\mathbf{b}|_k$  and  $|\mathbf{b}|_m$  may yield the same reconstructed phase differences. Essential for the remainder of the paper is only that we can assume the phase differences of the measurement samples within the small “isles” to be known.

In the second case, the relevant task is to stitch holographic sub-images which are, in themselves, fully coherent—the number of coherent observations  $C$  is here typically rather large. One can think of myriads of variations of such measurement setups, where the constant behavior of the reference signal source has to be known a priori or may even remain unknown but constant. One possible antenna measurement scenario, see Fig. 2(b), is to record two coherent sub-images for two installation locations of a receiving reference antenna.

### C. Phase Retrieval Formulations with Coherence Constraints

1) *A non-linear minimization problem:* The structuring of the  $C$  similar blocks is not yet visible in (6). Hence, we will explain the various newly introduced variables as shown in Fig. 1. The observation vector  $|\mathbf{b}_c| \in \mathbb{R}^M$  represents the  $c$ th block of the magnitude-only observations, composing the complete observation vector as, see Fig. 1,

$$|\mathbf{b}| = [|\mathbf{b}_1^T| \quad \dots \quad |\mathbf{b}_c^T| \quad \dots \quad |\mathbf{b}_C^T|]^T \quad (8)$$

with the corresponding forward-operators  $\mathbf{A}_c \in \mathbb{C}^{M \times N}$ . Here, the transpose is denoted by  $(\cdot)^T$ . Furthermore, we employ a reduced phase unknowns vector  $\boldsymbol{\psi} \in \mathbb{C}^M$  for the phase unknowns of  $|\mathbf{b}_1|$  only<sup>3</sup>. The phase differences to the  $c$ th block are implemented together with the observed magnitudes as a diagonal matrix with entries in the  $m$ th row and column

$$[\mathbf{B}_1]_{mm} = [|\mathbf{b}_1|]_m, \quad \mathbf{B}_1 \in \mathbb{R}^{M \times M}, \quad (9)$$

$$[\mathbf{B}_c]_{mm} = [|\mathbf{b}_c|]_m e^{j\Delta\phi_{m+cM,m}}, \quad \mathbf{B}_c \in \mathbb{C}^{M \times M}, \quad c \in \mathbb{N}^{[1, C-1]}, \quad (10)$$

leading to the overall block-structured matrix, see Fig. 1,

$$\mathbf{B} = [\mathbf{B}_1 \quad \mathbf{B}_2 \quad \dots \quad \mathbf{B}_c \quad \dots \quad \mathbf{B}_C]^T, \quad \mathbf{B} \in \mathbb{C}^{CM \times M} \quad (11)$$

including all observed phase differences and magnitudes. The  $M$  subgroups of observations are assembled in  $\mathbf{B}$ , where each column contains  $C$  entries including the observed phase differences. Furthermore, the  $m$ th column has an unknown phase  $[\boldsymbol{\psi}]_m$  for its complex entries.

<sup>3</sup>This choice is arbitrary and, due to the flexibility of the phase vector, has no influence on the solution or on the solution process at all.

These auxiliary quantities allow to rewrite (6) as

$$\min_{\psi, \mathbf{x}} \|\mathbf{A}\mathbf{x} - \mathbf{B}\psi\|_2 \quad \text{s. t. } |[\psi]_m| = 1 \text{ for } m \in \mathbb{N}^{[1, M]}. \quad (12)$$

This formulation is already much easier to implement than (6), since only one non-convex side constraint with reduced dimension remains. One simple trick to get rid of this side constraint is to replace the phase unknowns by the reconstructed observations in the manner of

$$\min_{\mathbf{x}} \left\| \begin{bmatrix} \mathbf{A}_1 \mathbf{x} & - & \mathbf{b}_1 \\ \mathbf{A}_2 \\ \vdots \\ \mathbf{A}_c \\ \vdots \\ \mathbf{A}_C \end{bmatrix} \mathbf{x} - \begin{bmatrix} \mathbf{B}_2 \\ \vdots \\ \mathbf{B}_c \\ \vdots \\ \mathbf{B}_C \end{bmatrix} \mathbf{B}_1^{-1} \mathbf{A}_1 \mathbf{x} \right\|_2. \quad (13)$$

Employing  $\psi = \mathbf{B}_1^{-1} \mathbf{A}_1 \mathbf{x}$  instead of  $|[\psi]_m| = 1$  as in (12) is an alternative kind of restriction. Its implications remain to be studied.

2) *A linear formulation for the original unknowns:* The non-linear side constraints (dependent on the type of solver, including a yet-to-determine weighting) and the additional  $\psi$  unknowns might be obstructive to deal with. Hence, we analyze under which circumstances a unique  $\psi$  exists — rendering the magnitude-one side constraint obsolete.

We proceed by looking at all the sub-equations of (12)

$$\mathbf{A}_c \mathbf{x} = \mathbf{B}_c \psi. \quad (14)$$

The matrices  $\mathbf{B}_c$  are diagonal with non-zero entries and, thus, invertible. Solving for  $\psi$  yields

$$\psi = \mathbf{B}_1^{-1} \mathbf{A}_1 \mathbf{x} = \dots = \mathbf{B}_c^{-1} \mathbf{A}_c \mathbf{x} = \dots = \mathbf{B}_C^{-1} \mathbf{A}_C \mathbf{x}, \quad (15)$$

which resembles a concatenation of generalized (pseudo-) eigenvalue problems [57]–[62] (with a known eigenvalue of value 1) and enables us to eliminate the phase unknowns from the problem by simultaneously solving  $C - 1$  generalized eigenvalue problems (with  $\kappa = 1$ ) in the form of

$$\mathbf{B}_1^{-1} \mathbf{A}_1 \mathbf{x} = \kappa \mathbf{B}_c^{-1} \mathbf{A}_c \mathbf{x} \quad \text{for } c \in \mathbb{N}^{[2, C]}. \quad (16)$$

Multiplying by the diagonal matrices  $\mathbf{B}_1 \mathbf{B}_c$  leads to

$$\mathbf{B}_c \mathbf{A}_1 \mathbf{x} = \mathbf{B}_1 \mathbf{A}_c \mathbf{x} \quad \text{for } c \in \mathbb{N}^{[2, C]}, \quad (17)$$

and allows to recast the overall problem as

$$\mathbf{Q}\mathbf{x} = \begin{bmatrix} \mathbf{B}_2 \mathbf{A}_1 - \mathbf{B}_1 \mathbf{A}_2 \\ \vdots \\ \mathbf{B}_c \mathbf{A}_1 - \mathbf{B}_1 \mathbf{A}_c \\ \vdots \\ \mathbf{B}_C \mathbf{A}_1 - \mathbf{B}_1 \mathbf{A}_C \end{bmatrix} \mathbf{x} = \mathbf{0} \quad (18)$$

with the matrix  $\mathbf{Q} \in \mathbb{C}^{M(C-1) \times N}$ .

Equation (18) is just the linear and homogeneous part of (13) multiplied by  $\mathbf{B}_1$  in order to avoid the division by potentially small  $\mathbf{B}$  entries and without the non-linear magnitude constraint  $|\mathbf{A}_1 \mathbf{x}| = |\mathbf{b}_1|$ . Having dropped the non-linear part of the constraints implies that not all information is employed in the source reconstruction. This may lead to a somewhat suboptimal solution, but with the benefit of solving

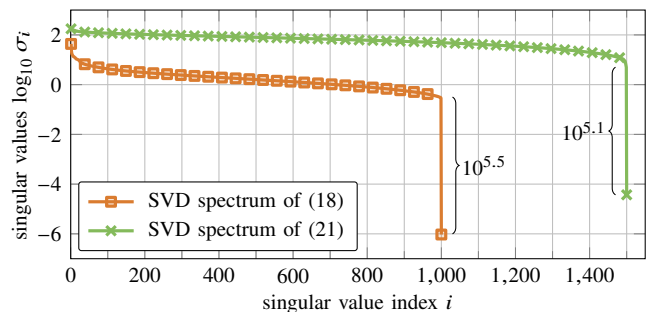


Figure 3. SVD spectra for a random matrix and random right-hand side, with  $N = 1000$ ,  $M = 1500$ ,  $C = 2$ , and  $n = 10^{-6}$ .

a linear system of equations — implying a huge improvement in reliability.

The properties of (18) are influenced by the properties of  $\mathbf{A}_c$ . We have assumed that  $\text{rk } \mathbf{A}_c = \min\{M, N\}$ . Hence, with a known  $\mathbf{x}$ ,  $\psi$  follows immediately. However, it is still unclear under which circumstances  $\mathbf{x}$  is unique.

Due to the block subtractions  $\mathbf{B}_c \mathbf{A}_1 - \mathbf{B}_1 \mathbf{A}_c$  in the matrix  $\mathbf{Q} \in \mathbb{C}^{M(C-1) \times N}$ , the true  $\mathbf{x}$  has to be in  $\ker \mathbf{Q}$ . We deduce a condition for a unique reconstruction: There has to be a non-trivial  $\ker \mathbf{Q}$  with  $\dim \ker \mathbf{Q} = 1$ . To fulfill this, we recall that  $\mathbf{Q}$  has  $N$  columns. Hence, for  $\dim \ker \mathbf{Q} = 1$ , it is required that  $\text{rk } \mathbf{Q} = N - 1$ . In order to yield this rank, a necessary but insufficient condition on the number of rows of the matrix  $\mathbf{Q}$  reads

$$M(C - 1) \geq N - 1. \quad (19)$$

A further requirement is that the eigenvalue  $\kappa = 1$  in the general eigenvalue problems (16) is unique, i.e., it is not degenerate. For the subtraction of two random Gaussian matrices, the probability of having the same degenerate eigenvalue approaches zero. For other matrices, this becomes more difficult to achieve, see the application example in Section V. For noisy observations, degenerate or near-degenerate eigenvectors may prevent a reliable reconstruction since the noisy observations are contained in the matrices  $\mathbf{B}_c$ . This is further discussed when noise is considered.

The task is now to determine the unique non-trivial vector in  $\ker \mathbf{A}_c$ . We consider the example of a Gaussian random  $\mathbf{A}$  and  $\mathbf{b}$  with  $N = 1000$ ,  $M = 1500$ ,  $C = 2$ , and a noise-to-signal ratio in the observation vector  $n = 10^{-6}$  according to

$$n = \frac{\|\mathbf{b}' - \mathbf{b}\|_2}{\|\mathbf{b}\|_2}, \quad (20)$$

where the primed vector  $\mathbf{b}'$  contains the noise-contaminated observations. The spectrum of the singular value decomposition (SVD) of  $\mathbf{Q} = \mathbf{U}\mathbf{S}\mathbf{V}^H$  is shown in Fig. 3. Exactly one noise-limited singular value with a magnitude of about  $10^{-6}$  is observed. In a magnitude-ordered SVD, we refer to this value as  $\sigma_N$ . The corresponding singular vector  $\mathbf{v}_N$  solves the phase-retrieval problem to a comparable accuracy level.

The task of finding the non-trivial vector in the null space can be tackled in different ways. The obvious one is to perform an SVD and pick the vector for the smallest singular value, but this is computationally rather expensive. From a complexity point of view, we can employ an iterative approach (preferably

a Krylov-subspace method, e.g., Arnoldi iterations [63]) to estimate the required SVD vector and scale the retrieved  $\mathbf{x}$  appropriately afterwards. Such an iteratively attained solution is also unique once the discussed conditions on  $\mathbf{Q}$  are fulfilled. Furthermore, it does not suffer from local minima, i.e., it is independent from the initial guess.<sup>4</sup> This is explained by the linearity (and, thus, convexity) of the formulation. Since the nullity of  $\mathbf{Q}$  is one, and (18) is a homogeneous linear system of equations, even standard solvers for linear systems of equations may be employed if we ensure that the trivial solution is avoided.

The formulation offers two possibilities to judge whether the reconstruction was successful. Firstly, a drop in the SVD spectrum between the smallest and the second smallest singular value should be observable. Secondly, the reconstructed phase vector  $\boldsymbol{\psi}$  according to (15) is required to have entries with constant magnitude. Unit-magnitude entries of the phase vector are to be created by a suitable scaling. If the magnitudes of the vector entries fluctuate a lot, the reconstruction was not successful.

3) *A linear formulation for the phase unknowns:* In the step from (10) to (11), the phase unknowns were replaced by  $\mathbf{x}$ . However, it is also possible the other way round. If  $\boldsymbol{\psi}$  is unique according to (19),  $\mathbf{x}$  may be replaced by the Moore-Penrose pseudo-inverse  $\mathbf{A}^+$  applied to the “complex” observations  $\mathbf{B}\boldsymbol{\psi}$  yielding again a linear null-space equation

$$\mathbf{R}\boldsymbol{\psi} = [\mathbf{A}\mathbf{A}^+\mathbf{B} - \mathbf{B}]\boldsymbol{\psi} = \mathbf{0} \quad (21)$$

with the matrix  $\mathbf{R} \in \mathbb{C}^{CM \times M}$ .

In Fig. 3, the spectrum of  $\mathbf{R} = \mathbf{U}\mathbf{S}\mathbf{V}^H$  is shown for a random matrix with  $N = 1000$  and  $n = 10^{-6}$ . Again, one singular vector  $\mathbf{v}_M$  of a non-trivial noise-limited null-space (with a singular value  $\sigma_M$ ) appears. While the null-space seems to have a numerically decreased dynamical range, the reconstruction quality is the same in this particular example. Whether one of the two versions is superior to the other is studied in the results sections. The main difference to (18) is found in the fact that the forward operator appears only in the form of the projector  $\mathbf{A}\mathbf{A}^+$ , removing any influence from the spectrum or null-space of  $\mathbf{A}$ .

After the reconstruction of  $\boldsymbol{\psi}$  by (21), the intuitive approach for the solution of the phaseless problem is to solve

$$\mathbf{A}\mathbf{x} = \mathbf{B}\boldsymbol{\psi} \quad (22)$$

in a subsequent step. This is done in the following unless stated otherwise. However, we have to keep in mind that the magnitude-one constraint in the reconstruction of  $\boldsymbol{\psi}$  was neglected for the sake of obtaining a linear system of equations. Since not all information is considered in the reconstruction process, the retrieved solution may be suboptimal. Instead of  $\mathbf{B}\boldsymbol{\psi}$ , the complex measurement vector may be reconstructed as

$$\mathbf{A}\mathbf{x} = \mathbf{B} \text{diag}(|\boldsymbol{\psi}|)^{-1} \boldsymbol{\psi} \quad (23)$$

enforcing the non-linear magnitude-one constraint.

<sup>4</sup>The initial guess is an important concept for non-convex minimization problems. Due to the possibility of local minima on the path to the global solution, it matters at which *initially guessed* vector the minimization starts.

#### 4) Discussion of the Linear Reconstruction Algorithms:

An important question is what happens if the conditions on  $\mathbf{Q}$  (or, equivalently,  $\mathbf{R}$ ) are not met. This might happen if the number of observations is not sufficiently large or if (near-) degenerate eigenvalues appear due to observation errors. Then, the numerically determined nullity  $\dim \ker \mathbf{Q}$  is greater than one. We still know that the true solution  $\mathbf{x} \in \ker \mathbf{Q}$ , but (18) or (21) alone are not sufficient anymore. This offers two strategies. Either the minimization problem is constraint by choosing only search vectors in  $\ker \mathbf{Q}$ , or the null-space equation is augmented by additional constraints. For instance, the phase vector constraints  $|\boldsymbol{\psi}_m| = 1$  may be included again. Another way to get rid of false solutions in  $\ker \mathbf{Q}$  for the homogeneous equation (18) is to fix the phase and the magnitude of up to  $C$  coherent (and hence complex) observations. As part of the following noise analysis, a single  $i$ th entry in  $\boldsymbol{\psi}$  is fixed in order to obtain the inhomogeneous and invertible linear system

$$\mathbf{R}_* \boldsymbol{\psi} = \mathbf{u}_{CM+1} \quad \text{with } \mathbf{R}_* = [\mathbf{R}^T \quad \mathbf{u}_i]^T \quad (24)$$

from (21), where  $\mathbf{u}_i$  refers to the  $i$ th unit vector.

5) *Influence of Measurement Errors on the Linear Reconstruction Algorithm:* We split the observations and the mapping inside the matrix  $\mathbf{B} = \mathbf{O}\mathbf{M}$  as

$$\mathbf{O} = \text{diag}([\mathbf{B}_1 \dots \mathbf{B}_C]), \quad (25)$$

$$\mathbf{M} = [\mathbf{I}_{M \times M} \dots \mathbf{I}_{M \times M}]^T, \quad (26)$$

where  $\mathbf{I}_{M \times M} \in \mathbb{R}^{M \times M}$  is an identity matrix. Assuming noisy measurements  $\mathbf{b}' = \mathbf{b} + \Delta\mathbf{b}$  leading to  $\mathbf{B}' = \mathbf{O}'\mathbf{M} = (\mathbf{O} + \Delta\mathbf{O})\mathbf{M} = \mathbf{B} + \Delta\mathbf{B}$ , we obtain

$$\|\Delta\mathbf{B}\|_F = \|\Delta\mathbf{O}\mathbf{M}\|_F \leq \|\Delta\mathbf{b}\|_F \sqrt{CM}, \quad (27)$$

where  $\|\cdot\|_F$  is the Frobenius norm. From the perturbation theory of linear systems, see for instance [64], applied to the homogeneous system in (21), we derive the upper bound

$$\frac{\|\Delta\boldsymbol{\psi}\|_F}{\|\boldsymbol{\psi}\|_F} \leq \|\mathbf{R}_*^{-1}\|_F \sqrt{CM} \|\mathbf{A}^+\mathbf{A} - \mathbf{I}_{CM \times CM}\|_F \|\Delta\mathbf{b}\|_F \quad (28)$$

to the relative error in  $\boldsymbol{\psi}$ . Thus, limited measurement noise has limited impact on the solution vector, proving the presented approach in (21) to be stable. Due to the similarities in the approaches, we expect a similar upper bound to hold true for (18). The stability of the reconstruction implies that if one unique singular value with value zero exists in the noiseless case, it does not become degenerate in the presence of noise.

#### D. State of the Art: Algorithms for Comparison

For the standard phase-retrieval problem (2), we consider the algorithms provided by PhasePack [2], [17], [19], [65]–[69]. The only generally applicable method for incorporating partial knowledge about phase differences, which may be employed to compare it with the proposed algorithm, is found in [7]. There, the structure of the forward operator is changed, leading to the non-linear non-convex minimization problem

$$\min_{\mathbf{x}} \left\| \left[ \begin{array}{c} \mathbf{A}_1 \\ \mathbf{A}_2 \\ \mathbf{A}_1 + \mathbf{A}_2 \\ \mathbf{A}_1 + j\mathbf{A}_2 \end{array} \right] \mathbf{x} - \left[ \begin{array}{c} |b_1| \\ |b_2| \\ |b_1 + b_2| \\ |b_1 + jb_2| \end{array} \right] \right\|_2, \quad (29)$$

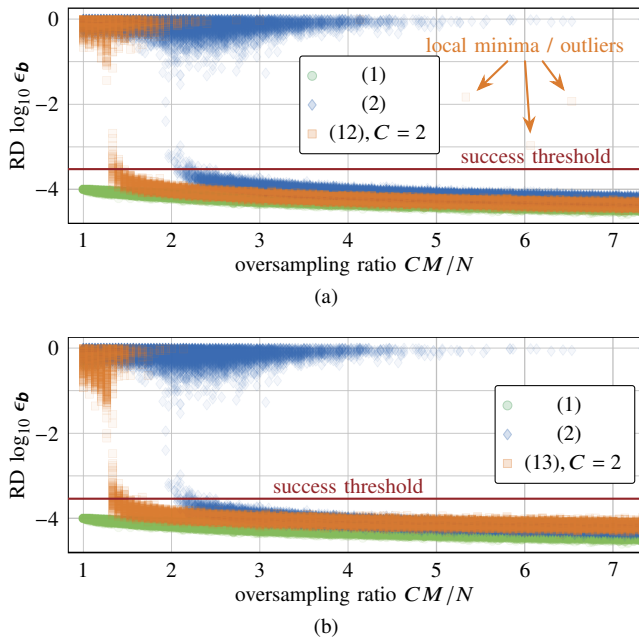


Figure 4. RD of the inverse problem solved for Gaussian random matrices,  $N = 30$ ,  $C = 2$ ,  $n = 10^{-4}$ . Each  $CM/N$ -ratio with 200 simulations. (a) Magnitude cost-functional minimization with reduced phase unknowns. (b) Magnitude cost-functional minimization with eliminated phase unknowns.

here given for the case  $C = 2$ . The phase-difference constraint is included in the cost functional and not written as an always-enforced side constraint. Of course, (29) can be rewritten for larger  $C$ .

#### IV. RESULTS FOR GAUSSIAN RANDOM MATRICES

The linear systems of equations are solved as described in Section III. Non-linear minimization problems are solved with the cost function minimizers provided by Matlab [70], where the active-set method is employed for the minimization with equality side constraints. Custom implementations for various solvers capable of handling problems of larger size have also been realized, based on the memory limited  $L$ -BFGS method [71], [72], by Broyden, Fletcher, Goldfarb, and Shannon. The initial guess  $\mathbf{x}_0$  for the non-linear solvers (6), (12), (13), and (29) is obtained by a spectral method according to [19]

$$\mathbf{x}_0 = \mathbf{v}_{\max} \frac{|\mathbf{b}^T \mathbf{A} \mathbf{v}_{\max}|}{\|\mathbf{A} \mathbf{v}_{\max}\|_2}, \quad (30)$$

with the eigenvector  $\mathbf{v}_{\max}$  corresponding to the largest eigenvalue of  $\mathbf{A}^H \mathbf{B}^H \mathbf{B} \mathbf{A}$ . The non-linear solvers rely heavily on the initial guess to avoid local minima. The solvers based on the null-space search—i.e., SVD-based ones and (24)—do not require an initial guess.

##### A. An Extensive Solver Comparison for $N = 30$

Considering  $N = 30$ , the phase reconstruction is performed for 200 random picks of  $\mathbf{A}$ , each with a randomly picked true solution  $\boldsymbol{\xi}$  and a corresponding right-hand side  $\mathbf{b} = \mathbf{A} \boldsymbol{\xi}$ . After the solution process, the true reconstruction deviation (RD)

$$\epsilon_{\mathbf{b}} = \|\mathbf{A} \mathbf{x} - \mathbf{A} \boldsymbol{\xi}\|_2 / \|\mathbf{A} \boldsymbol{\xi}\|_2 \quad (31)$$

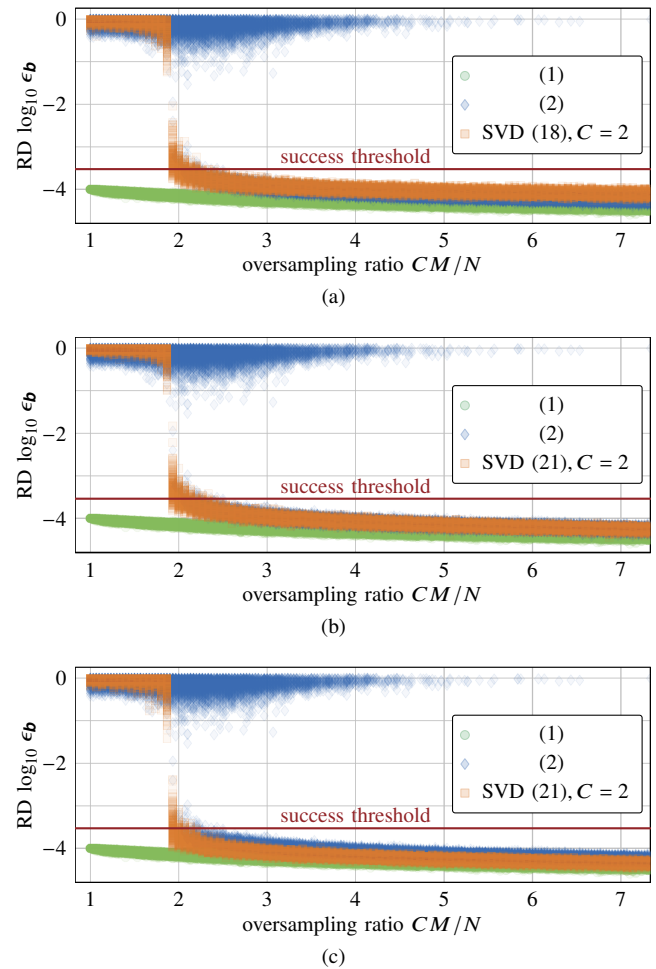


Figure 5. RD of the inverse problem solved for Gaussian random matrices,  $N = 30$ ,  $C = 2$ ,  $n = 10^{-4}$ . Each  $CM/N$ -ratio with 200 simulations. (a) First null-space search with SVD. (b) Second null-space search with SVD and fully linear reconstruction (22). (c) Second null-space search with SVD and enforced magnitude-one constraint (23).

is evaluated, where, however, the solution  $\mathbf{x}$  is obtained for a noise-contaminated vector  $\mathbf{b}'$  with the noise-to-signal ratio  $n$ .

For  $M \in \mathbb{N}^{[30, 220]}$  and  $n = 10^{-4}$ , the results are shown in Fig. 4(a) for the standard solver with phase (1), the standard magnitude-only solver (2), and the proposed solver with a  $C = 2$  phase-differences side constraint according to (12). The scatter plot provides the insight that the fully-coherent complex solver always works and the magnitude-only versions require a certain oversampling for a reliable reconstruction. We further observe that the solver with  $C = 2$  converges with fewer  $CM$ .

In Fig. 4(b), the fusion of magnitude-minimization and null-space condition (13) shows a better convergence than (12), with the main advantage of avoiding to get stuck in local minima for this scenario. In Fig. 5(a), the linear formulation, i.e., the null-space vector search, is included. The convergence behavior is slightly different. Almost exactly at  $CM/N = 58/30 \approx 1.93$  as expected, we observe a certain convergence. In contrast to Fig. 4(a), there are no outliers (i.e., local minima) above  $CM/N > 2$ . Unfortunately, the limit for successful reconstruction is a bit higher than in the other two cases. The second null-space equation (21) shows a

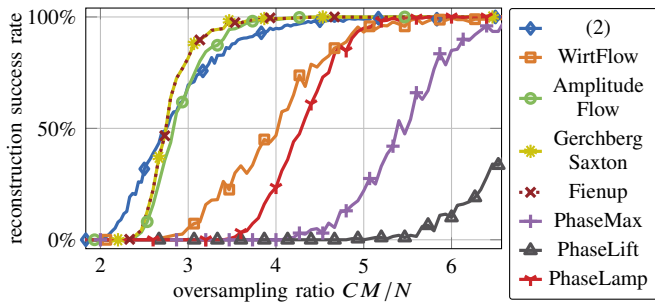


Figure 6. Success rate for Gaussian matrices,  $N = 30$ , noise  $n = 10^{-4}$ , and for the comparison  $CM/N = M/N$ , PhasePack solvers [67].

comparable behavior in Fig. 5(b) with slightly lower RDs. In Fig. 5(c), the magnitude-one constraint for the reconstructed phase unknowns is enforced according to (23). This seems to improve the RD if the reconstruction is working, i.e., if the success threshold  $CM/N \geq 58/30$  is fulfilled.

We introduce a threshold of  $3n$  with the noise-to-signal ratio  $n = 10^{-4}$  as defined in (20) and call a reconstruction with a RD below this limit *successful* and above *failed*. As seen in Figs. 4 and 5, this is a rather demanding definition of a successful reconstruction which excludes three kinds of solutions: global false solutions due to insufficient sampling, wrong solutions due to local minima, and almost acceptable solutions, where, e.g., the solver convergence was too slow.

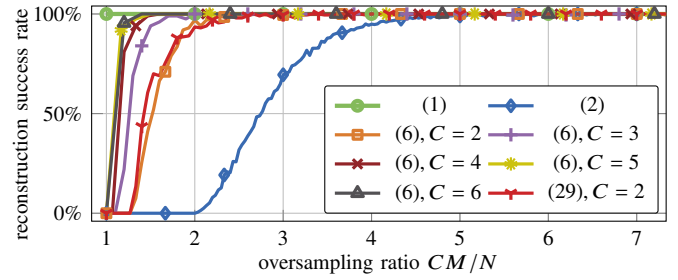
This allows us to introduce a success rate for the reconstruction. In Fig. 6, the minimization of (2) with the L-BFGS method is compared to many methods provided by PhasePack [67] and the simple cost function minimization is among the best-performing solvers. The complex solver (1) has a success rate of 100%. It is a reasonable choice that (29) (related to the comparison method for partially coherent phase retrieval) is minimized with the L-BFGS method in the following.

In Fig. 7(a), the required oversampling ratio  $CM/N$  for a high chance of success for the phase-difference solvers (6) moves towards a value of  $CM/N = 1$  with increasing  $C$ . The same is observed for (12) in Fig. 7(b). The standard phaseless solver (2) performs worst since it has the smallest knowledge about the inverse problem. The solver (13), which solves only for  $\mathbf{x}$ , performs better than the two previous versions.

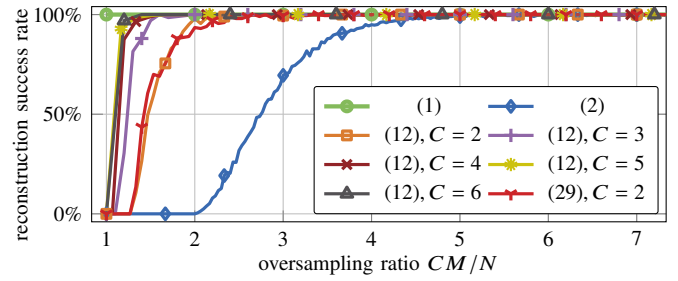
So far, the magnitude-only solvers, including the versions with partially coherent observations, have shown a rather good convergence rate — with a slight advantage of (12) over (6) and a great advantage for (13). However, for increasing  $M$ , local minima possibly prevent a 100% reconstruction rate. In Fig. 7(d), the SVD is employed to identify the vector for the smallest singular value in (18). As expected, the transition from failed to successful reconstruction occurs rather abruptly at around

$$CM/N \geq \frac{C(N-1)}{N(C-1)}, \quad (32)$$

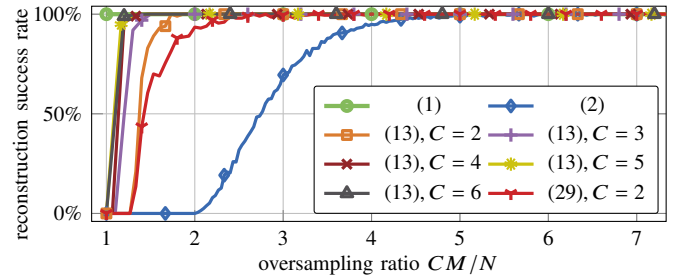
which is a recasted version of (19). The SVD-based solver (21) performs marginally better in the transition to a certain reconstruction in Fig. 7(e).



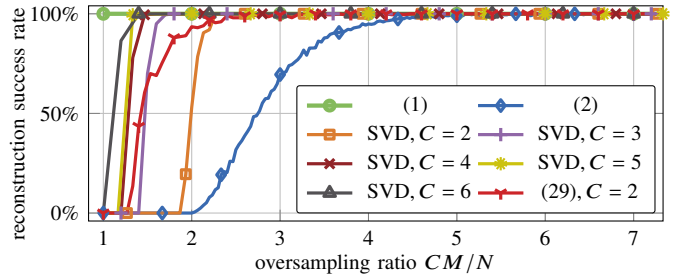
(a)



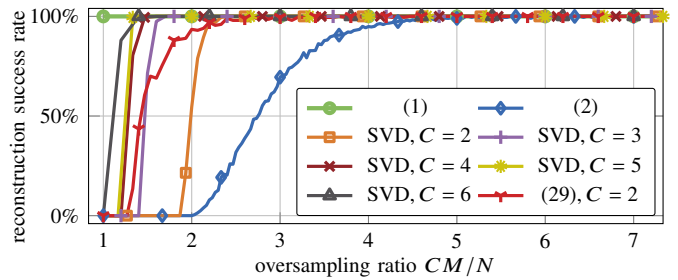
(b)



(c)



(d)



(e)

Figure 7. Success rate for Gaussian matrices,  $N = 30$ , noise level  $n = 10^{-4}$ , and for the comparison  $CM/N$ . (a) Different non-convex solvers (6) including phase unknowns. (b) Different non-convex solvers (12) including a reduced number of phase unknowns. (c) Different non-convex solvers (13) with eliminated phase unknowns. (d) Linearized solvers (18) with SVD. (e) Linearized solvers (21) with SVD.

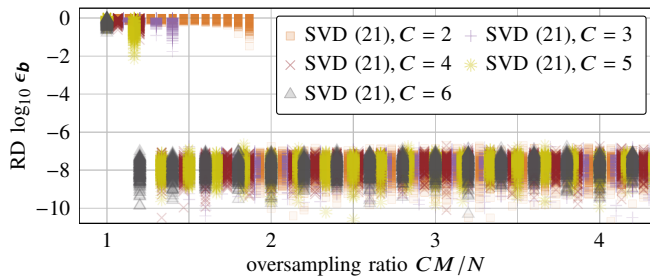


Figure 8. RD of the inverse problem solved for Gaussian random matrices,  $N = 30$ ,  $n = 0$ . Each  $CM/N$  ratio with 200 simulations.

The minimizations according to (6) and (12) never reach a certain reconstruction since they strongly depend on the initial guess, and sometimes the spectral method fails in this respect.

At an oversampling ratio where the minimizers come close to a success rate of 100%, the SVD null-space solutions are able to reach a certain reconstruction. The comparison method (29) is non-convex without guaranteed convergence and may get stuck in local minima, but empirically it performs here quite well. The downsides of this method become apparent later. Also, the minimization of (13) achieves certain reconstruction in the hitherto presented results.

Finally, we investigate the noise-free case, i.e.,  $n = 0$ , for the second null-space solver (21) in Fig. 8. The achievable accuracy is on average at around  $10^{-8}$  once the necessary oversampling criteria are met, e.g., at  $2M/N = 58/30$  for  $C = 2$ . All proposed phase retrieval algorithms gain reconstruction accuracy once the ideal noise-free case is considered. The accuracy of the cost-function minimizations of course depends on the stopping criteria for the iterative solver.

### B. A Larger Scenario with $N = 3000$

Now, the noise level is set to  $n = 10^{-2}$  and the number of unknowns is increased to  $N = 3000$ . Among the non-linear minimization techniques, we investigate only the hitherto best one, which is (13). The two SVD-based solvers were on par so far and we investigate just one of them. The success rates, again for a threshold of  $3n$ , are depicted for two solvers in Fig. 9. Two differences to the  $N = 30$  case are observed.

On the one hand, the SVD-based solver requires a slightly larger oversampling ratio for convergence than expected from the threshold according to (19). E.g., for  $C = 2$ , the threshold for a successful reconstruction is at  $CM/N = 1.996$ , but success is only observed at  $CM/N > 2$ . The reason is the interaction of a noise-induced transition period, compare Fig. 5 to Fig. 8, and the demanding success threshold of  $3n$ .

On the other hand, the cost-function minimization (13) shows a worse success rate than for the case  $N = 30$ . In particular, it suffers from local minima for this example; the same happens for the noise-free case and large  $N$ . If our goal is a certain reconstruction rate of 100%, only the linear solver in Fig. 9 beats the magnitude-only solver and the state-of-the-art solver (29). It becomes clear that the non-linear non-convex minimizations fail to ensure a correct reconstruction. The SVD-based solvers are able to provide absolute certainty

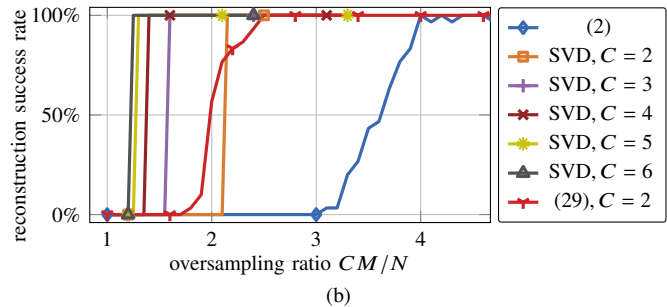
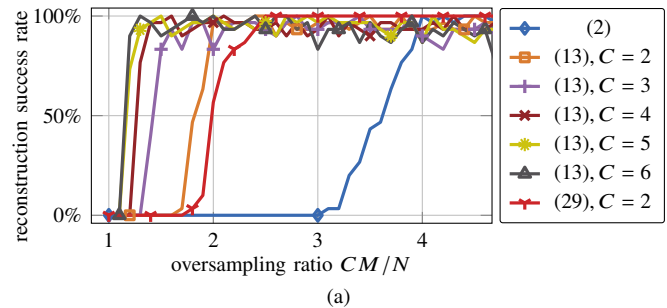


Figure 9. Success rate for Gaussian matrices,  $N = 3000$  and  $n = 10^{-2}$ , over  $CM/N$ . (a) Non-linear cost function solver (13). (b) SVD-solver (18).

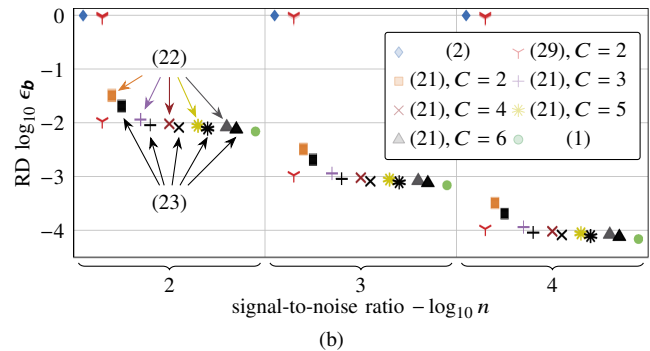
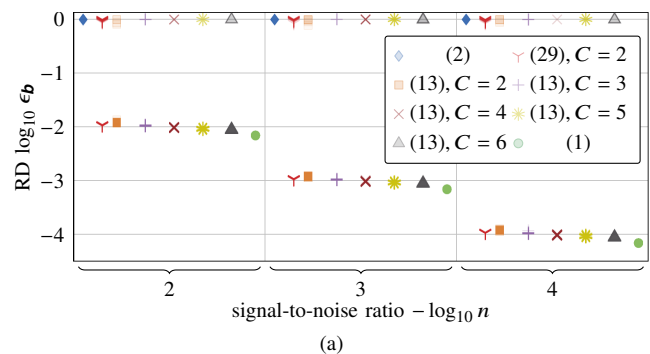


Figure 10. SNR analysis, 100 random simulations,  $N = 3000$ ,  $CM = 2.1N$ ,  $n \in \{10^{-2}, 10^{-3}, 10^{-4}\}$ . (a) Non-linear solver (13). (b) Linear solver (21) with phase reconstruction according to (22) and (23).

at the theoretically determined thresholds dependent on  $C$ , within a noise-caused margin over the expected threshold.

This influence of noise on the behavior of the non-linear solver (13) and the linear solver (21) is analyzed in Fig. 10 for  $N = 3000$ ,  $CM = 2.1N$ , 100 random simulations, and  $n \in \{10^{-2}, 10^{-3}, 10^{-4}\}$ . Comparison methods comprise the standard complex (best-performing) and phaseless (worst-performing, local minima) solvers and the multi-probe com-

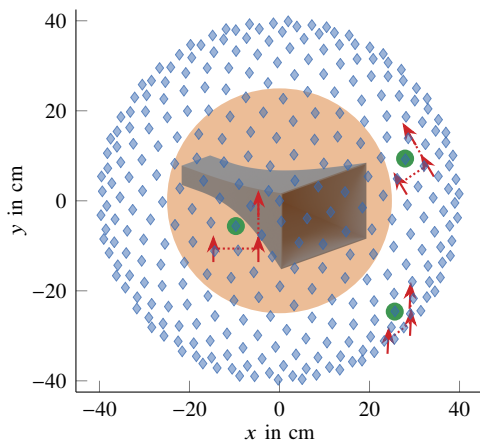


Figure 11. Synthetic antenna near-field measurement setup. An L-shaped probe array (red arrows) around the measurement reference position (green dot) is used to acquire magnitude and local phase difference information (here:  $C = 3$ ) at the sample locations (blue diamonds). The solution vector  $\mathbf{x}$  corresponds to surface currents densities placed tangentially on the smallest sphere (orange sphere) enclosing the horn antenna.

parison algorithm for  $C = 2$  (sometimes suffering from local minima). The performance of the partially-coherent phaseless solvers for  $C \in \mathbb{N}^{[2,6]}$  depends, as for all other solvers except for local minima, linearly on the chosen SNR. The linear method (21) with enforced magnitude-one constraints (23) reliably provides a good solution.

#### V. AN EXEMPLARY APPLICATION: PHASE RETRIEVAL FOR SYNTHETIC ANTENNA NEAR-FIELD MEASUREMENT DATA

We now consider a synthetic antenna near-field measurement setup as illustrated in Fig. 11. For more information on the idea of NFFFTs, for instance refer to [73]–[80]. As part of a phaseless NFFFT, the phases of the observed NFs are to be reconstructed. In the context of the setup in Fig. 11, the measurement vector  $|\mathbf{b}|$  corresponds to the signals received by known probe antennas placed at sample locations (blue diamonds) on a closed hull surrounding the antenna under test (AUT), which here is a horn antenna. In order to model the electromagnetic radiation of the AUT, the unknown coefficients  $\mathbf{x}$  of equivalent sources on an enclosing surface (orange sphere) are introduced. The received probe signals and the coefficients of the equivalent sources are linked via the electromagnetic radiation operator  $\mathbf{A}$ , which typically does not feature Gaussian distributed rows. Skipping the details — we refer the interested reader to [79]–[82] —, the spectrum of  $\mathbf{A}$  is strongly decaying and typically exhibits a non-trivial kernel, just to name two major differences to Gaussian matrices.

Assuming a probe antenna array and coherence between the probe elements, we are able to apply the presented phase retrieval algorithms. To pick reasonable multi-antenna probes, we recapitulate that this measurement setup and its field distributions are three-dimensional, but a two-dimensional description on the measurement surface is sufficient. Linking phases in two dimensions is possible in the case of a three-element probe array with an L-shape: Two linearly independent phase differences are acquired at every measurement location, resulting in  $C = 3$ . The L-probe (red arrows) placed

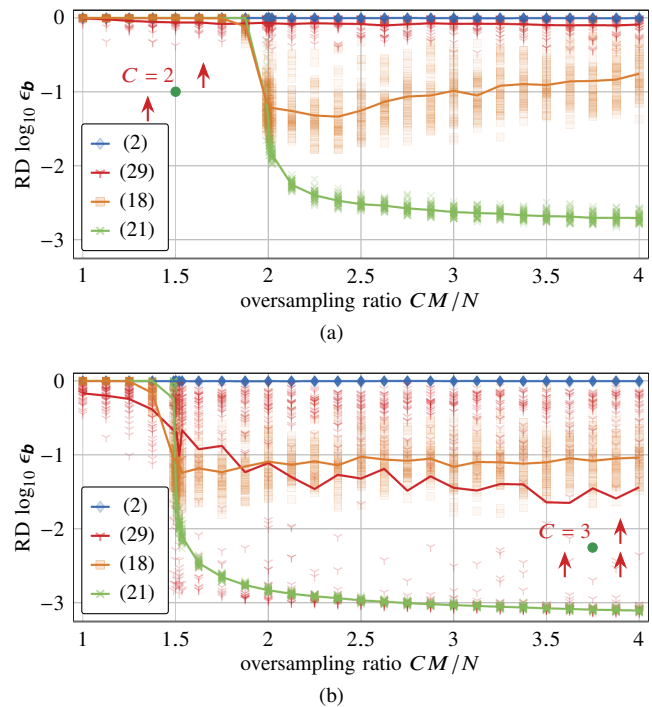


Figure 12. RD of the inverse problem solved for a synthetic antenna near-field measurement setup. The average logarithmic RD is indicated by the solid lines. (a) Utilizing only the two diagonal array elements of the L-shaped probe ( $C = 2$ ). (b) Employing a three-element, L-shaped probe array ( $C = 3$ ).

at an exemplary measurement location (green dot) is illustrated in Fig. 11. For a comparison case with  $C = 2$ , we pick the two diagonal probe elements only. Real-world measurement setups for such a scenario are found in [7], [32]–[36]. We stick to synthetic data since i) only simulated results offer the knowledge of the true solution and ii) studies on a large set of different antennas are not really feasible with measurements.

In the considered synthetic measurement setup, the equivalent-source sphere enclosing the AUT and a measurement sphere, exhibit diameters of  $5\lambda$  and  $8\lambda$ , respectively, where  $\lambda$  is the free-space wavelength. As equivalent sources,  $N = 1200$  tangential Hertzian dipoles are utilized and the horizontal as well as the vertical spacing between the probe-array elements is  $1\lambda$ . Each probe element is modeled as a single Hertzian dipole.

The obtainable RDs for the two known formulations (2) and (29), as well as the two proposed ones (21) and (18), is depicted in Fig. 12.

The described cases of  $C = 2$  and  $C = 3$  are given in Fig. 12(a) and (b), respectively. For every ratio of  $CM/N$ , 50 random orientations of the AUT were simulated, resulting in different measurement vectors. All results were obtained for a noise-to-signal ratio of  $n = 10^{-3}$ .

In both cases, the best results are obtained with formulation (21), which is observed to reliably yield accurate results above a certain ratio of  $CM/N$ . The existing formulations (2) and (29) are observed to either fail completely or they are not guaranteed to find a satisfactory solution. All formulations exploiting the phase differences are observed to yield better results for the case of the full L-shaped probe ( $C = 3$ ) compared to the two-element diagonal probe ( $C = 2$ ). Especially formu-

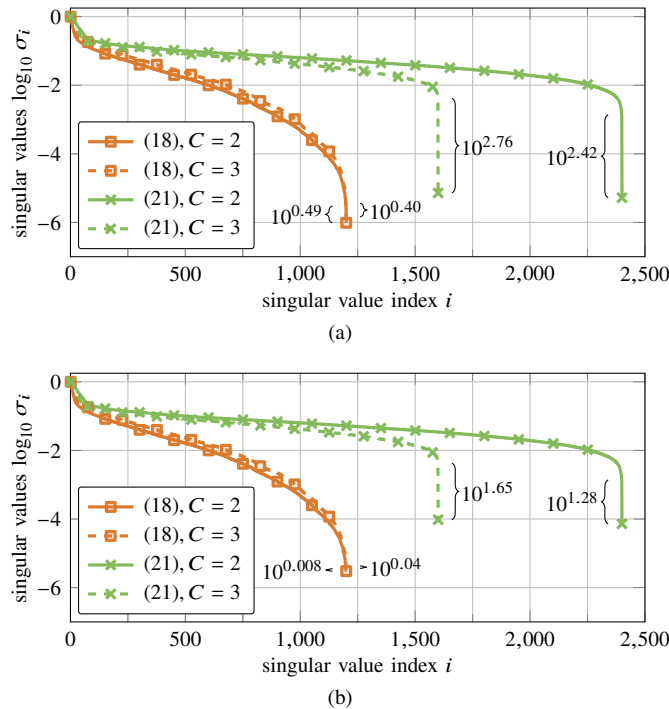


Figure 13. Normalized SVD spectra for  $\mathbf{Q}$  of (18) and  $\mathbf{R}$  of (21) for the cases  $C = 2$  and  $C = 3$  of the synthetic measurement data. (a) Noise-free case  $n = 0$ . (b) Noise-contaminated observations with  $n = 10^{-3}$ .

lation (29) is observed to benefit significantly. It yields similar results as (18) in the case of  $C = 3$ . The difference between the two proposed null-space formulations, (18) and (21), can be explained by looking at the spectrum of the singular values of  $\mathbf{Q}$  and  $\mathbf{R}$ . Considering a noise-free setup with  $CM/N = 3$  and the L-shaped probe, the spectra of  $\mathbf{Q}$  and  $\mathbf{R}$  are given in Fig. 13. The null-space is more distinct for (21), i.e., the ratio of the second smallest singular value to the smallest one is significantly greater for  $\mathbf{R}$  than for  $\mathbf{Q}$ .

Whenever perturbations affect the observations, and thus the spectrum of the singular values, it is more difficult to avoid false solutions and to maintain the desired null-space of  $\mathbf{Q}$ . Since  $\mathbf{R}$  features a more pronounced separation between its non-trivial null-space vector (smallest singular value) and false solutions (any other singular value), this formulation is more robust with respect to noise for the considered exemplary scenario and its forward operator.

## VI. CONCLUSION

Various formulations of the phase retrieval problem with additional knowledge of phase differences within subsets of observations have been presented. Two of the formulations are based on homogeneous linear systems of equations and require only defined oversampling and mild conditions to work with certainty.

Since the non-linear magnitude constraints are only implicitly fulfilled in these linear equations, they do not exploit the full available information and may be seen as *suboptimal yet simply reachable* solutions. In order to improve the solution obtained in particular for cases with insufficient oversampling, a minimization problem for a non-linear cost

functional has also been presented, which provides better results than comparable algorithms found in literature.

The presented results demonstrate that reliable phase retrieval for partially coherent observations is possible if certain conditions on the phase retrieval equations are fulfilled. Only for the case of a non-Gaussian forward operator, differences in the reconstruction behavior between the two SVD-based solvers are found. For the discussed scenario, it seems that (21) is preferable, in particular in the presence of noise.

## REFERENCES

- [1] Y. Shechtman, Y. C. Eldar, O. Cohen, H. N. Chapman, J. Miao, and M. Segev, "Phase retrieval with application to optical imaging: A contemporary overview," *IEEE Signal Process. Mag.*, vol. 32, no. 3, pp. 87–109, May 2015.
- [2] R. W. Gerchberg and W. O. Saxton, "A practical algorithm for the determination of phase from image and diffraction plane pictures," *Optik*, vol. 35, no. 2, pp. 237–246, 1972.
- [3] J. Miao, R. L. Sandberg, and C. Song, "Coherent X-ray diffraction imaging," *IEEE J. Sel. Topics Quantum Electron.*, vol. 18, no. 1, pp. 399–410, 2012.
- [4] F. Pfeiffer, T. Weitkamp, O. Bunk, and C. David, "Phase retrieval and differential phase-contrast imaging with low-brilliance X-ray sources," *Nat. Phys.*, vol. 2, no. 4, pp. 258–261, Apr. 2006.
- [5] T. Isernia, G. Leone, and R. Pierri, "Radiation pattern evaluation from near-field intensities on planes," *IEEE Trans. Antennas Propag.*, vol. 44, no. 5, pp. 701–710, May 1996.
- [6] R. G. Yaccarino and Y. Rahmat-Samii, "Phaseless bi-polar planar near-field measurements and diagnostics of array antennas," *IEEE Trans. Antennas Propag.*, vol. 47, no. 3, pp. 574–583, Mar. 1999.
- [7] A. Paulus, J. Knapp, and T. F. Eibert, "Phaseless near-field far-field transformation utilizing combinations of probe signals," *IEEE Trans. Antennas Propag.*, vol. 65, no. 10, pp. 5492–5502, Oct. 2017.
- [8] J. Knapp, A. Paulus, and T. F. Eibert, "Reconstruction of squared field magnitudes and relative phases from magnitude-only near-field measurements," *IEEE Trans. Antennas Propag.*, vol. 67, no. 5, pp. 3397–3409, May 2019.
- [9] W. Coene, G. Janssen, M. O. de Beeck, and D. van Dyck, "Phase retrieval through focus variation for ultra-resolution in field-emission transmission electron microscopy," *Phys. Rev. Lett.*, vol. 69, no. 26, pp. 3743–3746, Dec. 1992.
- [10] H. M. L. Faulkner and J. M. Rodenburg, "Movable aperture lensless transmission microscopy: A novel phase retrieval algorithm," *Phys. Rev. Lett.*, vol. 93, no. 2, p. 023903, Jul. 2004.
- [11] M. Guizar-Sicairos and J. R. Fienup, "Phase retrieval with transverse translation diversity: A nonlinear optimization approach," *Opt. Express*, vol. 16, no. 10, pp. 7264–7278, May 2008.
- [12] E. J. Candès, X. Li, and M. Soltanolkotabi, "Phase retrieval from coded diffraction patterns," *Appl. Comput. Harmonic Anal.*, vol. 39, no. 2, pp. 277–299, Sep. 2015.
- [13] J. Bacca, S. Pinilla, and H. Arguello, "Super-resolution phase retrieval from designed coded diffraction patterns," *IEEE Trans. Image Process.*, vol. 29, pp. 2598–2609, 2020.
- [14] M. A. Iwen, A. Viswanathan, and Y. Wang, "Fast phase retrieval from local correlation measurements," *SIAM J. Imaging Sci.*, vol. 9, no. 4, pp. 1655–1688, 2016.
- [15] T. Ramos, B. E. Grønager, M. S. Andersen, and J. W. Andreasen, "Direct three-dimensional tomographic reconstruction and phase retrieval of far-field coherent diffraction patterns," *Phys. Rev. A*, vol. 99, no. 2, p. 023801, Feb. 2019.
- [16] N. Sissouno, F. Boßmann, F. Filbir, M. Iwen, M. Kahnt, R. Saab, C. Schroer, and W. zu Castell, "A direct solver for the phase retrieval problem in ptychographic imaging," *Math. Comput. Simulation*, vol. 176, pp. 292–300, Oct. 2019.
- [17] E. J. Candès, T. Strohmer, and V. Voroninski, "Phaselift: Exact and stable signal recovery from magnitude measurements via convex programming," *Commun. Pure Appl. Math.*, vol. 66, no. 8, pp. 1241–1274, 2013.
- [18] E. J. Candès, Y. C. Eldar, T. Strohmer, and V. Voroninski, "Phase retrieval via matrix completion," *SIAM Rev.*, vol. 57, no. 2, pp. 225–251, 2015.

- [19] E. J. Candes, X. Li, and M. Soltanolkotabi, "Phase retrieval via Wirtinger flow: Theory and algorithms," *IEEE Trans. Inf. Theory*, vol. 61, no. 4, pp. 1985–2007, Apr. 2015.
- [20] P. Netrapalli, P. Jain, and S. Sanghavi, "Phase retrieval using alternating minimization," *IEEE Trans. Signal Process.*, vol. 63, no. 18, pp. 4814–4826, Sep. 2015.
- [21] P. Grohs and M. Rathmair, "Stable gabor phase retrieval for multivariate functions," *arXiv preprint arXiv:1903.01104*, 2019.
- [22] M. A. Iwen, S. Merhi, and M. Perlmutter, "Lower lipschitz bounds for phase retrieval from locally supported measurements," *Appl. Comput. Harmonic Anal.*, vol. 47, no. 2, pp. 526–538, 2019.
- [23] C. Cheng, I. Daubechies, N. Dym, and J. Lu, "Stable phase retrieval from locally stable and conditionally connected measurements," *arXiv preprint arXiv:2006.11709*, 2020.
- [24] P. Grohs, S. Koppensteiner, and M. Rathmair, "Phase retrieval: Uniqueness and stability," *SIAM Rev.*, vol. 62, no. 2, pp. 301–350, 2020.
- [25] V. Pohl, F. Yang, and H. Boche, "Phaseless signal recovery in infinite dimensional spaces using structured modulations," *J. Fourier Anal. Appl.*, vol. 20, no. 6, pp. 1212–1233, 2014.
- [26] C. H. Schmidt and Y. Rahmat-Samii, "Phaseless spherical near-field antenna measurements: Concept, algorithm and simulation," in *Proc. IEEE Antennas Propag. Soc. Int. Symp. (APSURSI)*, Charleston, SC, USA, Jun. 2009.
- [27] K. Jaganathan, S. Oymak, and B. Hassibi, "Sparse phase retrieval: Uniqueness guarantees and recovery algorithms," *IEEE Trans. Signal Process.*, vol. 65, no. 9, pp. 2402–2410, May 2017.
- [28] E. J. R. Pauwels, A. Beck, Y. C. Eldar, and S. Sabach, "On Fienup methods for sparse phase retrieval," *IEEE Trans. Signal Process.*, vol. 66, no. 4, pp. 982–991, Feb. 2018.
- [29] T. Qiu and D. P. Palomar, "Undersampled sparse phase retrieval via majorization–minimization," *IEEE Trans. Signal Process.*, vol. 65, no. 22, pp. 5957–5969, Nov. 2017.
- [30] G. Wang, L. Zhang, G. B. Giannakis, M. Akcakaya, and J. Chen, "Sparse phase retrieval via truncated amplitude flow," *IEEE Trans. Signal Process.*, vol. 66, no. 2, pp. 479–491, Jan. 2018.
- [31] G. Baechler, M. Krekovic, J. Ranieri, A. Chebira, Y. M. Lu, and M. Vetterli, "Super resolution phase retrieval for sparse signals," *IEEE Trans. Signal Process.*, vol. 67, no. 18, pp. 4839–4854, Sep. 2019.
- [32] S. Costanzo, G. Di Massa, and M. D. Migliore, "Integrated microstrip probe for phaseless near-field measurements on plane-polar geometry," *Electron. Lett.*, vol. 37, no. 16, pp. 1018–1020, Aug. 2001.
- [33] S. Costanzo and G. Di Massa, "An integrated probe for phaseless plane-polar near-field measurements," *Microw. Opt. Technol. Lett.*, vol. 30, no. 5, pp. 293–295, 2001.
- [34] S. Costanzo, G. Di Massa, and M. D. Migliore, "A novel hybrid approach for far-field characterization from near-field amplitude-only measurements on arbitrary scanning surfaces," *IEEE Trans. Antennas Propag.*, vol. 53, no. 6, pp. 1866–1874, Jun. 2005.
- [35] S. Costanzo and G. Di Massa, "Wideband phase retrieval technique from amplitude-only near-field data," *Radioengineering*, vol. 17, no. 4, pp. 8–12, 2008.
- [36] R. Tena-Sánchez, M. Sierra-Castañer, and L. J. Foged, "Relative phase reconstruction based on multiprobe solutions and post-processing techniques," in *Proc. Eur. Conf. Antennas Propag.*, Copenhagen, DK, Mar. 2020.
- [37] A. Paulus, J. Knapp, J. Kornprobst, and T. F. Eibert, "Improved-reliability phase-retrieval with broadband antenna measurements," in *Proc. Eur. Conf. Antennas Propag.*, Copenhagen, DK, Mar. 2020.
- [38] J. Knapp, A. Paulus, J. Kornprobst, U. Siart, and T. F. Eibert, "Multi-frequency phase retrieval for antenna measurements," *IEEE Trans. Antennas Propag.*, 2020 (early access).
- [39] V. Pohl, F. Yang, and H. Boche, "Phase retrieval from low-rate samples," *Sampling Theory Signal Image Process.*, vol. 14, pp. 71–99, 2015.
- [40] G. Junkin, T. Huang, and J. C. Bennett, "Holographic testing of terahertz antennas," *IEEE Trans. Antennas Propag.*, vol. 48, no. 3, pp. 409–417, Mar. 2000.
- [41] G. Castaldi and I. M. Pinto, "Well-posed well-conditioned phase retrieval technique using a known reference source," in *Proc. IEEE Antennas Propag. Soc. Int. Symp. USNC/URSI Nat. Radio Sci. Meeting*, Salt Lake City, UT, USA, Jul. 2000, pp. 1780–1782.
- [42] J. Laviada and F. Las-Heras, "Phaseless antenna measurement on non-redundant sample points via Leith-Upatnieks holography," *IEEE Trans. Antennas Propag.*, vol. 61, no. 8, pp. 4036–4044, Aug. 2013.
- [43] J. Laviada Martinez, A. Arboleya, Y. Alvarez-Lopez, C. Garcia-Gonzalez, and F. Las-Heras, "Phaseless antenna diagnostics based on off-axis holography with synthetic reference wave," *IEEE Antennas Wireless Propag. Lett.*, vol. 13, pp. 43–46, 2014.
- [44] A. Arboleya, J. Laviada, J. Ala-Laurinaho, Y. Alvarez, F. Las-Heras, and A. V. Räsänen, "Phaseless characterization of broadband antennas," *IEEE Trans. Antennas Propag.*, vol. 64, no. 2, pp. 484–495, Feb. 2015.
- [45] A. Arboleya, J. Laviada, and F. Las-Heras, "Scalar calibration for broadband phaseless antenna measurements based on indirect off-axis holography," *IEEE Trans. Antennas Propag.*, no. 6, pp. 3241–3246, Jun. 2018.
- [46] R. Tena-Sánchez and M. Sierra-Castañer, "Evaluation of software defined radio receiver for phaseless near-field measurements," in *Proc. 40th Ann. Meeting Symp. Antenna Meas. Techn. Assoc. (AMTA)*, Williamsburg, VA, USA, Nov. 2018.
- [47] P. Berlt, C. Bornkessel, and M. A. Hein, "Accurate 3D phase recovery of automotive antennas through LTE power measurements on a cylindrical surface," in *Proc. Eur. Conf. Antennas Propag.*, Copenhagen, DK, Apr. 2020.
- [48] D. Gabor, "Microscopy by reconstructed wave-fronts," in *Proc. R. Soc. Lond. A*, vol. 197, 1949, pp. 454–487.
- [49] E. N. Leith and J. Upatnieks, "Reconstructed wavefronts and communication theory," *J. Opt. Soc. America*, vol. 52, no. 10, pp. 1123–1130, Oct. 1962.
- [50] D. A. Barmherzig, J. Sun, P.-N. Li, T. J. Lane, and E. J. Candès, "Holographic phase retrieval and reference design," *Inverse Problems*, vol. 35, no. 9, p. 094001, 2019.
- [51] A. Viswanathan and M. Iwen, "Fast angular synchronization for phase retrieval via incomplete information," in *Wavelets Sparsity XVI*, vol. 9597. International Society for Optics and Photonics, 2015, p. 959718.
- [52] T. Gao and Z. Zhao, "Multi-frequency phase synchronization," *arXiv preprint arXiv:1901.08235*, 2019.
- [53] M. A. Iwen, B. Preskitt, R. Saab, and A. Viswanathan, "Phase retrieval from local measurements: Improved robustness via eigenvector-based angular synchronization," *Appl. Comput. Harmonic Anal.*, vol. 48, no. 1, pp. 415–444, 2020.
- [54] R. M. Goldstein, H. A. Zebker, and C. L. Werner, "Satellite radar interferometry: Two-dimensional phase unwrapping," *Radio Sci.*, vol. 23, no. 4, pp. 713–720, 1988.
- [55] D. C. Ghiglia and M. D. Pritt, "Two-dimensional phase unwrapping: Theory, algorithms, and software," *Hoboken, NJ, US: John Wiley & Sons*, Apr. 1998.
- [56] V. Pohl, H. Boche, and C. Yapar, "Modulated wideband converter for compressive phase retrieval of bandlimited signals," in *Proc. Int. ITG Conf. Syst. Commun. Coding*, Hamburg, Germany, Feb. 2017.
- [57] K.-C. Toh and L. N. Trefethen, "Calculation of pseudospectra by the arnoldi iteration," *SIAM J. Sci. Comput.*, vol. 17, no. 1, pp. 1–15, 1996.
- [58] L. N. Trefethen, "Pseudospectra of linear operators," *SIAM Rev.*, vol. 39, no. 3, pp. 383–406, 1997.
- [59] —, "Pseudospectra of matrices," *Numer. Anal.*, vol. 91, pp. 234–266, 1991.
- [60] G. Boutry, M. Elad, G. H. Golub, and P. Milanfar, "The generalized eigenvalue problem for nonsquare pencils using a minimal perturbation approach," *SIAM J. Matrix Anal. Appl.*, vol. 27, no. 2, pp. 582–601, 2005.
- [61] D. Chu and G. H. Golub, "On a generalized eigenvalue problem for nonsquare pencils," *SIAM J. Matrix Anal. Appl.*, vol. 28, no. 3, pp. 770–787, 2006.
- [62] D. Kressner, E. Mengi, I. Nakić, and N. Truhar, "Generalized eigenvalue problems with specified eigenvalues," *IMA J. Numer. Anal.*, vol. 34, no. 2, pp. 480–501, Apr. 2014.
- [63] W. E. Arnoldi, "The principle of minimized iterations in the solution of the matrix eigenvalue problem," *Q. Appl. Math.*, vol. 9, no. 1, pp. 17–29, Apr. 1951.
- [64] J. W. Demmel, *Applied Numerical Linear Algebra*. Society for Industrial and Applied Mathematics, 1997.
- [65] J. R. Fienup, "Phase retrieval algorithms: A comparison," *Appl. Opt.*, vol. 21, no. 15, pp. 2758–2769, 1982.
- [66] H. Zhang and Y. Liang, "Reshaped Wirtinger flow for solving quadratic system of equations," in *Proc. Adv. Neural Inf. Process. Syst.* 29, Barcelona, Spain, Dec. 2016, pp. 2622–2630.
- [67] R. Chandra, Z. Zhong, J. Hontz, V. McCulloch, C. Studer, and T. Goldstein, "PhasePack: A phase retrieval library," in *Proc. 51st Asilomar Conf. Signals Syst. Comput.*, Pacific Grove, CA, USA, Oct. 2017, pp. 1617–1621.
- [68] O. Dhifallah, C. Thrampoulidis, and Y. M. Lu, "Phase retrieval via polytope optimization: Geometry, phase transitions, and new algorithms," *arXiv preprint arXiv:1805.09555*, 2018.
- [69] T. Goldstein and C. Studer, "Phasemax: Convex phase retrieval via basis pursuit," *IEEE Trans. Inf. Theory*, vol. 64, no. 4, pp. 2675–2689, Apr. 2018.

- [70] MATLAB, *version 9.7.0 (R2019b) Update 2*. Natick, MA, USA: The MathWorks Inc., 2019. [Online]. Available: <https://www.mathworks.com/>
- [71] D. C. Liu and J. Nocedal, "On the limited memory BFGS method for large scale optimization," *Math. Program.*, vol. 45, no. 1, pp. 503–528, Aug. 1989.
- [72] J. Nocedal and S. J. Wright, *Numerical Optimization*, 2nd ed. New York, NY, USA: Springer Science+Business Media, 2006.
- [73] A. Ludwig, "Near-field far-field transformations using spherical-wave expansions," *IEEE Trans. Antennas Propag.*, vol. 19, no. 2, pp. 214–220, Feb. 1971.
- [74] J. E. Hansen, *Spherical Near-Field Antenna Measurements*. London, UK: Peter Pelegrinus Ltd., 1988.
- [75] T. K. Sarkar and A. Taaghoul, "Near-field to near/far-field transformation for arbitrary near-field geometry utilizing an equivalent electric current and MoM," *IEEE Trans. Antennas Propag.*, vol. 47, no. 3, pp. 566–573, Mar. 1999.
- [76] Y. Álvarez, F. Las-Heras, and M. R. Pino, "Reconstruction of equivalent currents distribution over arbitrary three-dimensional surfaces based on integral equation algorithms," *IEEE Trans. Antennas Propag.*, vol. 55, no. 12, pp. 3460–3468, Dec. 2007.
- [77] C. H. Schmidt, M. M. Leibfritz, and T. F. Eibert, "Fully probe-corrected near-field far-field transformation employing plane wave expansion and diagonal translation operators," *IEEE Trans. Antennas Propag.*, vol. 56, no. 3, pp. 737–746, Mar. 2008.
- [78] M. A. Qureshi, C. H. Schmidt, and T. F. Eibert, "Efficient near-field far-field transformation for nonredundant sampling representation on arbitrary surfaces in near-field antenna measurements," *IEEE Trans. Antennas Propag.*, vol. 61, no. 4, pp. 2025–2033, Apr. 2013.
- [79] J. L. Araque Quijano and G. Vecchi, "Field and source equivalence in source reconstruction on 3D surfaces," *Prog. Electromagn. Res.*, vol. 103, pp. 67–100, 2010.
- [80] J. Kornprobst, R. A. M. Mauermayer, O. Neitz, J. Knapp, and T. F. Eibert, "On the solution of inverse equivalent surface-source problems," *Prog. Electromagn. Res.*, vol. 165, pp. 47–65, 2019.
- [81] N. Bleistein and J. K. Cohen, "Nonuniqueness in the inverse source problem in acoustics and electromagnetics," *J. Math. Physics*, vol. 18, no. 2, pp. 194–201, 1977.
- [82] T. B. Hansen, A. Paulus, and T. F. Eibert, "On the condition number of a normal matrix in near-field to far-field transformations," *IEEE Trans. Antennas Propag.*, vol. 67, no. 3, pp. 2028–2033, Mar. 2019.